Civil Engineering Beyond Limits 4 (2026) 11154
Civil Engineering Beyond Limits
journal home: www.acapublishing.com/journals/1/cebel

Research Article

Progressive Collapse and Structural Resistance Assessment of Code-Compliant High-Ductility Steel MRFs under NBCC and ASCE 7

Alireza Mirzaei[1], Khosrow Bargi[*,1]
[1]School of Civil Engineering, College of Engineering, University of Tehran, Tehran, Iran

Keywords

Progressive collapse,
Pushdown analysis,
Nonlinear pushover analysis,
High-ductility steel moment-resisting frames,
ASCE 7-22, NBCC 2020.

Abstract

Although extensive research has been conducted on the seismic and progressive collapse behavior of steel moment-resisting frames (MRFs), limited attention has been given to the influence of different seismic design provisions on the resistance of these systems against progressive collapse. This study investigates the progressive collapse resistance of high-ductility MRFs designed according to the seismic requirements of ASCE 7-22 and NBCC 2020. Three-, six-, and nine-story archetype frames were designed using ETABS in accordance with AISC 360-22/AISC 341-22 and CSA S16-19 requirements. The designed structures were subsequently modeled in OpenSees using concentrated plasticity elements and validated nonlinear modeling procedures. Nonlinear pushover analyses were performed to evaluate key seismic performance parameters, including overstrength, ductility, stiffness, and plastic hinge development. In addition, nonlinear pushdown analyses were conducted under interior- and exterior-column removal scenarios following the GSA guidelines to assess structural resistance against progressive collapse. The results indicate that frames designed according to NBCC 2020 generally exhibit larger member sizes, higher steel consumption, greater initial stiffness, and higher lateral and vertical load-carrying capacities than their ASCE 7-22 counterparts. Consequently, NBCC-designed frames develop larger overstrength factors and substantially greater progressive collapse resistance. In contrast, ASCE-designed frames demonstrate higher ductility and deformation capacity under seismic loading. Plastic hinge distributions indicate that the intended strong-column weak-beam mechanism was achieved in most archetypes. Overall, the results demonstrate that column location plays a critical role in progressive collapse behavior, with interior-column removal leading to substantially higher collapse resistance and more stable post-yield response compared with exterior-column removal.

1. Introduction

Steel Moment Resisting Frames (MRFs) are among the most widely used structural systems for modern buildings due to their high ductility and reliable seismic performance. By utilizing rigid beam-to-column connections capable of developing significant inelastic deformations, these systems can effectively dissipate seismic energy and maintain structural stability under severe earthquake excitations. Consequently, current seismic design provisions place considerable emphasis on ensuring adequate strength, stiffness, and ductility of MRFs to achieve satisfactory performance during strong ground motions. However, recent catastrophic events have highlighted that structural safety should not be evaluated solely based on resistance to conventional design loads. Buildings may also be subjected to abnormal loading scenarios such as explosions, vehicle impacts, fire, construction or design errors, and other accidental or intentional hazards that are generally not considered in routine structural design. Such extreme events may trigger localized damage through the loss of a critical structural component, leading to a redistribution of internal forces throughout the structure. If the remaining structural system lacks sufficient robustness, continuity, and alternate load paths, the initial local failure may propagate progressively, resulting in partial or even total collapse of the building. This phenomenon, commonly referred to as progressive collapse, has become an important consideration in performance-based structural design and resilience assessment. Therefore, evaluating the capability of steel MRFs to sustain local damage while preventing disproportionate collapse has emerged as a critical research topic for enhancing the overall safety and robustness of building structures.

Due to the widespread application of MRFs in seismic regions and the growing concern regarding their robustness under extreme loading scenarios, numerous studies have been conducted to investigate their structural behavior and collapse resistance. Flores et al. [1] investigated the influence of gravity framing systems on the collapse performance of steel special moment frames and demonstrated that gravity-frame continuity and connection properties significantly enhance collapse resistance. Özhendekci et al. [2] investigated the seismic performance of 10-story steel MRFs with different span arrangements and found that span-to-story height ratios greater than 2.5 increase structural vulnerability by causing larger story drifts and plastic rotations under severe earthquakes. Aslani et al. [3] proposed a hybrid rotational friction damper combined with SMA cables for steel moment-resisting frames and demonstrated that the system significantly reduces inter-story drifts and residual deformations while enhancing seismic resilience under both DBE and MCE ground motions. Flores et al. [4] assessed floor acceleration demands in steel special moment frames considering different modeling assumptions and showed that gravity framing systems and connection characteristics can significantly influence peak floor accelerations and the seismic demands imposed on nonstructural components. Shi et al. [5] experimentally investigated the cyclic behavior of high-performance weathering steel connections in moment-resisting frames and demonstrated that these connections exhibit stable hysteretic responses, adequate ductility, and seismic performance comparable to conventional steel connections. Heshmati et al. [6] evaluated MRFs systems using FEMA P695 under near and far field records

*Corresponding Author: kbargi@ut.ac.ir
Received 14 Jun 2026; Revised 09 Jul 2026; Accepted 15 Jul 2026
https://doi.org/10.36937/cebel.2026.11154
2687-5756 /© 2022 The Authors, Published by ACA Publishing; a trademark of ACADEMY Ltd. All rights reserved.

and found that near-field earthquakes increase collapse probability while MRF systems provide higher safety margins and better collapse performance. Jayarajan [7] assessed the seismic performance of steel moment-resisting frames with partial-strength connections and found that properly designed semi-rigid connections provide sufficient ductility to satisfy the drift limits prescribed by modern seismic design codes. Lignos et al. [8] evaluated the collapse behavior of steel moment frames through full-scale shake table tests at the E-Defense facility and demonstrated that enhancing column flexural strength and delaying local buckling can substantially increase structural collapse capacity. Galvis et al. [9] assessed the seismic performance of pre-Northridge welded steel moment frame buildings and developed a framework for quantifying structural damage, economic losses, and post-earthquake recovery, highlighting their implications for community resilience.

Given the importance of structural robustness against localized damage, numerous studies have focused on the progressive collapse resistance and the mechanisms governing load redistribution following the loss of critical structural members. Kim et al. [10] investigated the progressive collapse resistance of steel moment frames using pushdown analysis and found that increasing the number of stories and spans enhances collapse resistance, whereas longer span lengths reduce the load-carrying capacity after column loss. Liu et al. [11] investigated the seismic and progressive collapse performance of prefabricated RCS frame structures and showed that the incorporation of tendons and Y-shaped braces significantly enhances lateral strength and collapse resistance under both central and exterior column removal scenarios. Li et al. [12] investigated the progressive collapse resistance of three-dimensional steel frames with reinforced concrete floor slabs under an interior column removal scenario and demonstrated that floor slabs substantially enhance structural stiffness and load-carrying capacity through composite action. Song et al. [13] experimentally investigated the progressive collapse behavior of fully bonded prestressed precast concrete frames under a middle-column removal scenario and found that flexural action, compressive arch action, and catenary action collectively contribute to collapse resistance at different deformation stages. Elshaer et al. [14] evaluated the progressive collapse performance of multistory reinforced concrete buildings subjected to seismic actions and showed that column loss during earthquakes is more critical than under gravity loading, while floor slabs significantly enhance collapse resistance through catenary action. Al-Salloum et al. [15] developed a practical numerical procedure to investigate the progressive collapse behavior of reinforced concrete high-rise buildings and demonstrated its applicability by analyzing a typical RC tower subjected to blast-induced loading scenarios. Zhao et al. [16] investigated the progressive collapse behavior of single-layer latticed domes under different loading conditions and demonstrated that loss of a critical member can trigger snap-through collapse due to localized joint failure despite the high structural redundancy.

Although numerous studies have investigated the seismic and progressive collapse behavior of steel moment-resisting frames, limited research has focused on the influence of different seismic design codes on the resistance of these systems against progressive collapse. In particular, a comprehensive comparison between high-ductility steel moment-resisting frames designed according to the seismic provisions of ASCE 7-22 [17] and NBCC 2020 [18] has not been sufficiently addressed in the existing literature. To address this gap, the present study evaluates the seismic and progressive collapse performance of high-ductility steel moment-resisting frames designed based on the loading requirements of ASCE 7-22 and NBCC 2020, and detailed according to the provisions of AISC 360-22 [19], AISC 341-22 [20], and CSA S16-19 [21]. The structural models were first designed in ETABS [22] and subsequently developed in OpenSees [23] for nonlinear analyses. Pushover and pushdown analyses were conducted to assess the seismic response and structural resistance under column-removal scenarios. The findings of this study provide a basis for evaluating how different seismic design provisions influence the overall performance and progressive collapse resistance of steel moment-resisting frames.

2. Seismic Design Procedure and Archetype Development

In this study, high-ductility steel moment-resisting frames (MRFs) were designed according to the seismic provisions of both the United States and Canadian design standards in order to evaluate the influence of different code requirements on seismic performance and progressive collapse resistance. For the U.S. design approach, the seismic design and detailing requirements were adopted from AISC 341-22 and AISC 360-22, while the Canadian archetypes were designed in accordance with CSA S16-19. Seismic loading was determined based on ASCE 7-22 and NBCC 2020 for the U.S. and Canadian designs, respectively.

High-ductility steel moment-resisting frames are among the most widely used seismic force-resisting systems due to their ability to dissipate large amounts of earthquake energy through stable inelastic deformations. The seismic design philosophy of these systems is based on the development of plastic hinges at predetermined locations, primarily at both ends of beams, while undesirable inelastic behavior in other structural components should be prevented. To achieve this objective, the strong-column weak-beam requirement prescribed by the aforementioned standards was strictly enforced during the design process. This design criterion ensures that yielding is concentrated in beam elements, thereby promoting a desirable global collapse mechanism and enhancing the overall ductility and energy dissipation capacity of the structure. Since the archetype structures were intended to represent buildings located in regions of high seismicity, the seismic design parameters adopted in this study are summarized in Table 1. To provide a consistent basis for comparing the seismic design provisions of ASCE 7-22 and NBCC 2020, the building models were designed under representative high-seismicity conditions using comparable design assumptions. As summarized in Table 1, both design cases were assigned Site Class D and Seismic Design Category D (4), while the selected spectral acceleration parameters correspond to high seismic hazard conditions according to the respective code provisions. These common design assumptions were adopted to establish a consistent basis for comparing the influence of the two design frameworks on the seismic and progressive-collapse performance of the steel moment-resisting frames.

Table 1. Seismic design parameters adopted for the archetype structures

Parameter	ASCE 7-22	NBCC 2020
Structural system	Special Moment Frame (SMF)	Ductile Moment-Resisting Frame (D-MRF)
Site class	D	D
Seismic design category	D	SC4
Importance factor (I_e)	1.0	1.0
Response modification factor	R = 8.0	R_d = 5.0
Overstrength factor	Ω = 3.0	R_o = 1.5
Deflection amplification factor	C_d = 5.5	R_dR_o = 7.5
Design spectral parameters	S_{DS} = 1.0 g	$S_a(0.2)$ = 1.0 g
	S_{D1} = 0.6 g	$S_a(0.5)$ = 0.8 g
	S_{MS} = 1.5 g	$S_a(1.0)$ = 0.6 g
	S_{M1} = 0.9 g	$S_a(2.0)$ = 0.35 g

The approximate fundamental period used for seismic design was determined according to the empirical expressions specified by each code. For the ASCE 7-22 provisions, the approximate period was calculated using Eq. (1), whereas Eq. (2) was adopted according to NBCC 2020:

$$T_a = 0.0724h^{0.8} \tag{1}$$

$$T_a = 0.085h^{0.75} \tag{2}$$

where T_a is the approximate fundamental period of the structure and h is the total structural height measured from the base to the roof level (m).

To avoid unconservative estimation of seismic forces, both design standards impose an upper limit on the analytical fundamental period. According to ASCE 7-22, the calculated period shall not exceed $1.4T_a$, whereas NBCC 2020 limits the period to $1.5T_a$.

For the U.S. design procedure, the seismic base shear was determined according to Eq. (3):

$$V = C_s W \tag{3}$$

where V is the design base shear, W is the effective seismic weight of the structure, and Cs is the seismic response coefficient. For the considered structures, $C_s = S_a/RI_e$, where Sa is the design spectral acceleration corresponding to the fundamental period, R is the response modification coefficient, and Ie is the importance factor. For high-ductility steel moment-resisting frames designed according to ASCE 7-22, a response modification factor of R = 8 was adopted.

According to NBCC 2020, the design base shear was calculated using Eq. (4):

$$V = \frac{S(T_a)M_v I_e W}{R_d R_o} \tag{4}$$

where $S(T_a)$ is the design spectral acceleration at the fundamental period, Mv is the higher-mode factor accounting for the influence of higher vibration modes on the base shear (M_v = 1), Ie is the importance factor, and W is the effective seismic weight. The parameter Rd represents the ductility-related force modification factor, reflecting the capacity of the structure to dissipate energy through inelastic cyclic behavior, while Ro denotes the overstrength-related force modification factor accounting for the dependable reserve strength of the structural system. For ductile steel moment-resisting frames, values of R_d = 5.0 and R_o = 1.5 were adopted in accordance with NBCC 2020. It should be noted that both ASCE 7-22 and NBCC 2020 specify upper and lower limits for the design base shear, which were satisfied for all archetype structures considered in this study.

To investigate the influence of seismic design provisions, three-, six-, and nine-story archetype frames were designed independently according to both U.S. and Canadian code requirements. As illustrated in Figure 1, all structures were based on a regular square plan consisting of four bays in each principal direction with a bay length of 6.6 m. The seismic force-resisting system comprised steel moment-resisting frames in the Y-direction and concentrically braced frames in the X-direction. A constant story height of 4.0 m was considered for all archetypes.

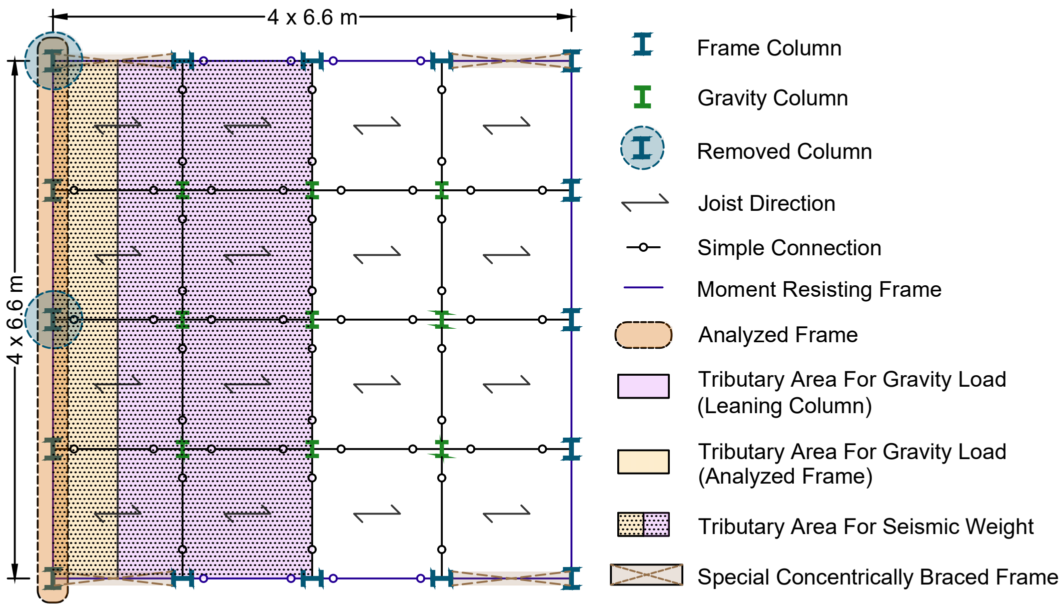

Figure 1. Plan configuration, structural layout, and tributary gravity loading used for the archetype models

Both the design and nonlinear analyses were conducted using two-dimensional frame models. Owing to the regularity and symmetry of the floor plan, this modeling approach provides an efficient and sufficiently accurate representation of the global structural response. To account for the gravity load contribution and second-order effects, a leaning-column modeling technique was adopted. The tributary gravity loads associated with the analyzed frame and the corresponding P–Δ effects transferred to the leaning column are illustrated in Figure 1.

All structural members were designed using ASTM A992 Grade 50 steel with a nominal yield strength of F_y = 345 MPa. The archetype structures were designed in ETABS, and the final beam and column sections obtained for both design standards are summarized in Table 2 and Table 3. For brevity, the elevation view of the three-story archetype frame and its corresponding loading details are shown in Figure 2, which are representative of all considered archetype structures. ASTM A992 Grade 50 steel and W-sections were consistently adopted for both ASCE 7-22 and NBCC 2020 designs to ensure a direct comparison of the resulting structural performance.

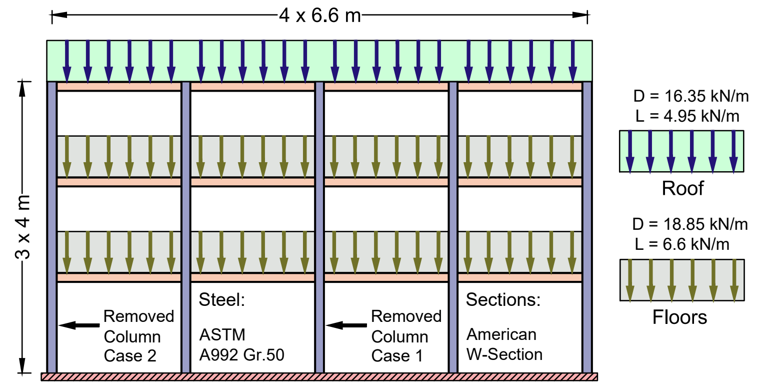

Figure 2. Elevation view of the three-story archetype frame and corresponding loading details

For high-ductility steel moment-resisting frames, story drift limitation is generally one of the governing design criteria. In the present study, drift requirements controlled the design of most archetype structures. According to ASCE 7-22, the amplified story drift obtained by applying the deflection amplification factor (C_d) shall not exceed 2% of the story height. Similarly, NBCC 2020 limits the story drift amplified by the factor R_dR_o/I_e to 2.5% of the story height. Figure 3 presents the drift profiles of all archetype structures and confirms that the drift requirements were satisfied in every case. Furthermore, the results indicate that the maximum drift demand generally occurs in the intermediate stories, which is consistent with the expected behavior of steel moment-resisting frames.

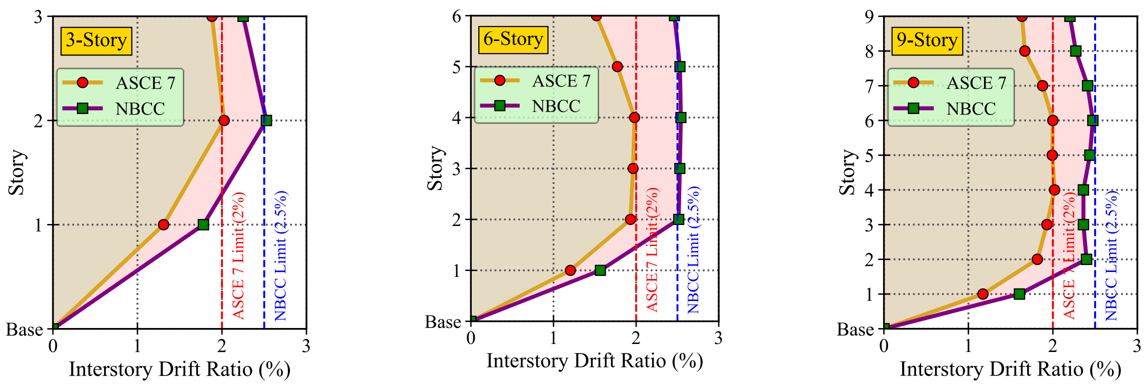

Figure 3. Comparison of elastic story drift ratios for the archetype frames designed based on ASCE and NBCC provisions

Figure 4 compares the distribution of design story shear forces along the height of the archetype frames designed according to ASCE 7-22 and NBCC 2020. As observed, the three-story frame designed based on ASCE 7-22 exhibits slightly higher story shear demands than its NBCC counterpart throughout the building height. In contrast, for the six- and nine-story archetypes, the NBCC-designed frames generally develop larger story shear forces at most floor levels. Overall, the differences become more pronounced as the structural height increases, reflecting the distinct procedures adopted by the two standards for estimating seismic design forces and period-dependent response parameters.

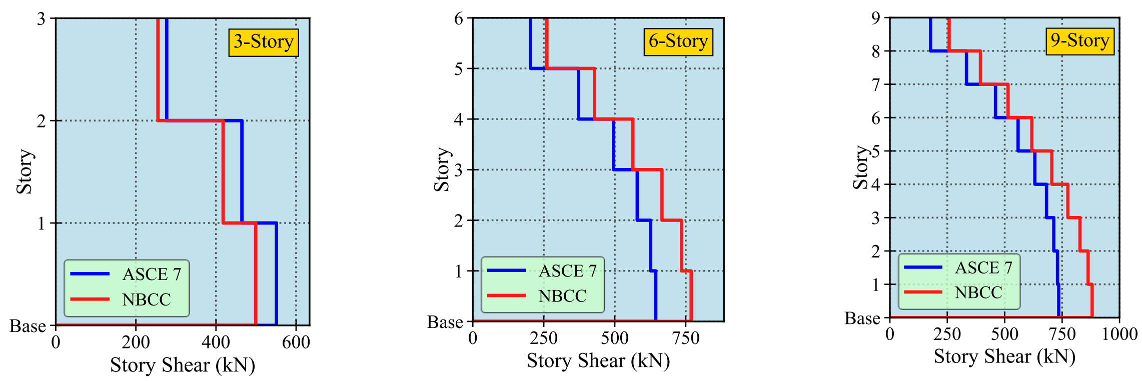

Figure 4. Story shear force profiles for the archetype frames designed based on ASCE 7-22 and NBCC 2020

Figure 5 compares the total structural steel weight of the archetype frames designed according to ASCE 7-22 and NBCC 2020. As can be observed, the archetypes designed based on NBCC 2020 consistently require a larger amount of structural steel than those designed according to ASCE 7-22. For all considered building heights, the steel consumption of the NBCC-designed frames is approximately 1.5 times that of the corresponding ASCE-designed frames.

Table 2. Design member sections of archetypes designed according to ASCE 7-22

Model	No. of Story	Beams	Columns
3-Story	1	W18X35	W16X89
	2	W18X40	W16X77
	3	W14X26	W12X96
6-Story	1	W21X44	W14X145
	2	W21X50	W14X145
	3	W21X50	W14X132
	4	W21X44	W12X120
	5	W18X40	W12X120
	6	W12X35	W12X96
9-Story	1	W21X44	W14X159
	2	W24X55	W14X159
	3	W21X50	W14X159
	4	W21X50	W14X159
	5	W18X55	W14X159
	6	W18X50	W14X132
	7	W18X40	W14X132
	8	W16X40	W14X132
	9	W12X22	W14X68

Table 3. Design member sections of archetypes designed according to NBCC 2020

Model	No. of Story	Beams	Columns
3-Story	1	W18X35	W14X159
	2	W18X55	W14X159
	3	W16X40	W12X96
6-Story	1	W21X44	W14X283
	2	W24X62	W14X283
	3	W21X62	W14X257
	4	W21X50	W14X233
	5	W18X60	W14X145
	6	W12X35	W12X120
9-Story	1	W21X44	W14X342
	2	W24X94	W14X342
	3	W24X76	W14X283
	4	W24X76	W14X283
	5	W21X73	W14X257
	6	W21X73	W14X211
	7	W21X68	W14X159
	8	W21X44	W14X159
	9	W16X40	W14X109

The differences observed in the member sizes and steel consumption between the ASCE 7 and NBCC designs can be largely attributed to the drift-control provisions specified by the two standards. According to NBCC 2020, the elastic story drift must be amplified by the factor $R_d R_o$, which is equal to $5.0 \times 1.5 = 7.5$ for ductile steel moment-resisting frames, and the resulting drift is limited to 2.5% of the story height. In contrast, ASCE 7-22 amplifies the elastic drift using the $C_d = 5.5$ and limits the amplified drift to 2% of the story height. Consequently, the effective drift amplification-to-drift limit ratio is approximately $7.5/2.5 = 3.0$ for NBCC and $5.5/2.0 = 2.75$ for ASCE 7. This indicates that the Canadian provisions impose a more demanding drift-control requirement, leading to larger member sections and, therefore, higher steel consumption in the NBCC-designed archetypes. Another reason for the differences between the two design approaches is the treatment of the fundamental period in drift evaluation. ASCE 7-22 permits the use of the analytical period, which may lead to lower seismic forces when the calculated period exceeds the empirical estimate. In contrast, NBCC 2020 limits the period used for drift calculations in ductile moment-resisting frames to 2.0 s, resulting in higher seismic demands, particularly for taller buildings. Consequently, the Canadian provisions generally lead to a more conservative design.

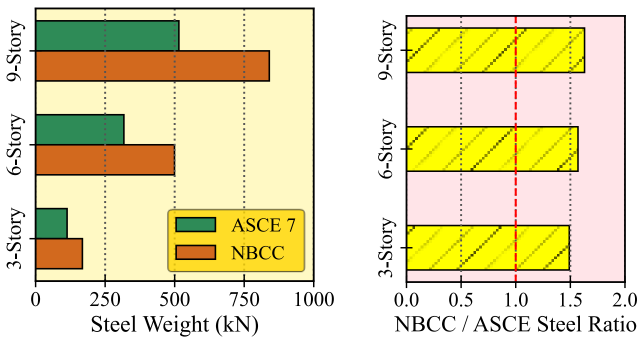

Figure 5. Comparison of structural steel weight for the archetype frames designed according to ASCE 7-22 and NBCC 2020

3. Numerical Modeling and Validation

Following the completion of the structural design process in ETABS, nonlinear analytical models were developed in OpenSees to evaluate the seismic and progressive collapse behavior of the archetype structures. The geometric and mechanical properties of the designed frames were extracted from the ETABS models and subsequently incorporated into the OpenSees environment.

A concentrated plasticity formulation was adopted to represent the nonlinear response of structural members [24]. As shown in Figure 6, each beam and column was modeled using an elastic beam-column element to capture the elastic stiffness and force distribution along the member length, while nonlinear rotational springs were assigned at both ends to simulate inelastic flexural behavior. This modeling strategy assumes that yielding and damage are concentrated within localized plastic hinge regions near the member ends, whereas the remaining portion of the member remains essentially elastic throughout the analysis.

The nonlinear rotational springs were defined using the Modified Ibarra–Medina–Krawinkler (IMK) deterioration model available in OpenSees through the IMKBilin material formulation. The deterioration framework originally proposed by Ibarra et al. [25] was subsequently refined by Lignos and Krawinkler [26,27] through extensive calibration against a large experimental database of steel wide-flange beam tests. In the present study, the modeling parameters were determined using the predictive equations proposed by Lignos and Krawinkler [26] and later updated by Hartloper and Lignos [28].

To incorporate gravity load effects and second-order response, leaning columns were introduced into the numerical models. These elements were modeled using elastic beam-column members with very large axial stiffness to ensure numerical stability during nonlinear analysis and negligible flexural stiffness to prevent participation in the lateral force-resisting system, while pinned end connections were assigned. In addition, one-half of the seismic mass associated with the building plan was applied as concentrated floor loads to the leaning column at each story level. Consequently, the leaning columns carried the tributary gravity loads and reproduced the global P–Δ effects without contributing to the lateral resistance of the structural system. This simplified modeling approach has been widely adopted in previous progressive-collapse studies; therefore, the conclusions of this study are limited to the global response of the analyzed two-dimensional frame models.

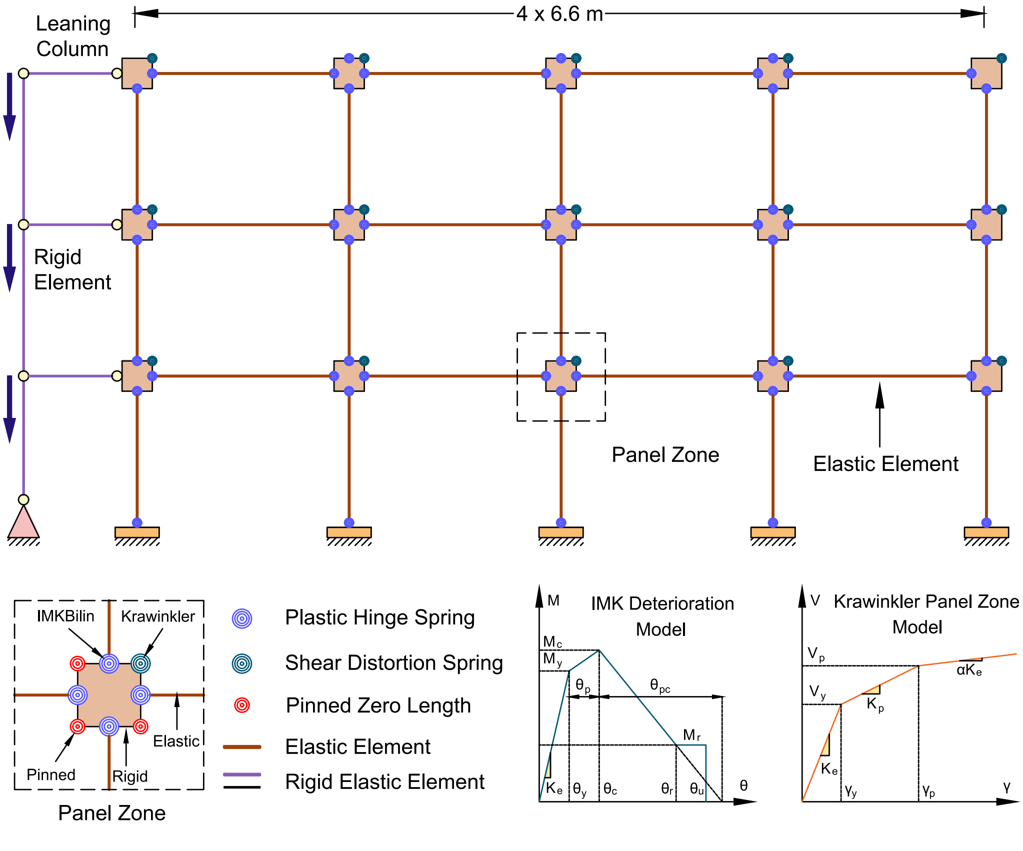

Figure 6. Schematic representation of the nonlinear frame model, including plastic hinges, panel zones, and leaning columns.

The shear deformation of beam-column joint regions was explicitly considered through the use of a rectangular panel zone model (Krawinkler) [24]. As illustrated in Figure 6, the panel zone was represented using a dedicated assemblage of rigid elements and nonlinear shear springs capable of simulating the inelastic shear behavior that develops within the joint core under seismic loading. The constitutive properties of the panel zone components were determined in accordance with the recommendations provided in NIST provisions [24] and current seismic design specifications, allowing both elastic and inelastic joint deformations to be captured during the analyses.

Regarding geometric transformation definitions, beam elements were assigned the Linear transformation, whereas column elements were modeled using the PDelta transformation to explicitly capture geometric nonlinearity arising from axial force effects. Consequently, large-displacement beam effects are beyond the scope of the adopted modeling approach, and the results should be interpreted accordingly.

To verify the accuracy and reliability of the adopted nonlinear modeling approach, a validation study was conducted using the two-story steel moment-resisting frame (2RSA) reported in the NIST GCR 10-917-8 [29]. The numerical model was developed in OpenSees following the same modeling procedures described in the previous paragraph. The geometric configuration and modeling details of the reference frame are presented in Figure 7(a). A nonlinear pushover analysis was subsequently performed, and the resulting capacity curve was compared with the corresponding reference results reported in NIST GCR 10-917-8. As illustrated in Figure 7(b), the pushover curve obtained from the OpenSees model shows excellent agreement with the reference response throughout both the elastic and inelastic ranges. The initial elastic stiffness is almost identical, with an error of less than 0.1%. Furthermore, the normalized peak base shear (V/W) predicted by the reference model is 0.415, compared with 0.41 obtained from the present model, demonstrating excellent agreement in peak strength. Furthermore, both models reach an ultimate roof drift ratio of approximately 6%, while exhibiting essentially the same normalized base shear level at the final stage of the response. These results confirm that the adopted modeling strategy can accurately reproduce the nonlinear response of steel moment-resisting frames and provide confidence in its application for the seismic and progressive-collapse analyses performed in this study.

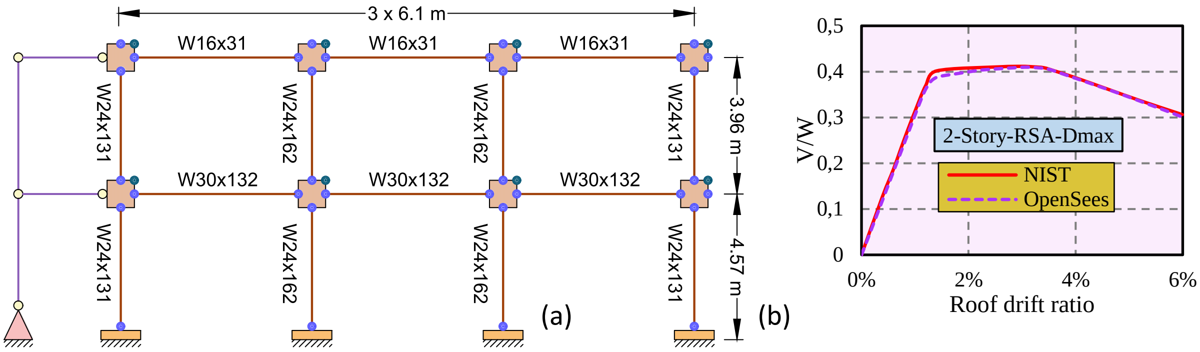

Figure 7. (a) geometry and modeling details of the reference two-story frame, (b) comparison of pushover curves obtained from the reference frame and the OpenSees model.

4. Nonlinear Assessment Methodology

4.1. Nonlinear pushover analysis

Nonlinear static pushover analysis was performed to evaluate the seismic capacity, strength characteristics, and inelastic deformation behavior of the archetype frames. This analysis procedure is widely used to investigate the progression of structural yielding, identify the sequence of plastic hinge formation, and estimate the global deformation capacity of structural systems under increasing lateral loading. By gradually increasing the applied lateral forces until a target displacement or structural instability is reached, the relationship between base shear and roof displacement can be established in the form of a capacity curve.

Prior to the application of lateral loads, gravity loads were applied and maintained throughout the analysis in accordance with the recommendations of the FEMA P695 [30] methodology. The gravity load combination adopted for the pushover analysis consisted of the dead load plus 0.25 times the live load. After the gravity-load analysis reached equilibrium, a monotonically increasing lateral load pattern was imposed on the structure. The lateral force distribution was determined using the first-mode force pattern, in which the force at each story was taken proportional to the product of the effective seismic mass and the corresponding first-mode shape amplitude. This loading pattern enables the dominant dynamic characteristics of the structure to be reasonably represented within a nonlinear static framework.

The seismic performance parameters were evaluated following the methodology proposed in FEMA P695. For this purpose, the pushover curves were normalized by the effective seismic weight of the structure, and the resulting capacity curves were expressed in terms of the base shear coefficient (V/W), where V denotes the base shear resistance and W represents the effective seismic weight. Based on the normalized pushover response, the system overstrength factor (Ω) was determined as the ratio between the maximum base shear capacity (V_{max}) and the design base shear (V_d). In addition, the period-based ductility factor (μ_T), which represents the deformation capacity of the structure beyond first yielding, was calculated as the ratio of the ultimate roof displacement (δ_u) to the effective yield displacement ($\delta_{y,eff}$). The δu corresponds to the point on the pushover curve where the lateral resistance decreases to 80% of the Vmax. The effective yield displacement was determined using Eq. (5).

$$\delta_{y,eff} = C_0 \frac{V_{max}}{W}\left[\frac{g}{4\pi^2}\right](max(T,T_1))^2 \quad (5)$$

where g is the gravitational acceleration, T is the code-based fundamental period used for design, and T_1 is the fundamental period obtained from modal analysis. The coefficient C_0 relates the displacement of the equivalent single-degree-of-freedom system to the roof displacement of the multi-degree-of-freedom structure and was calculated using Eq. (6).

$$C_0 = \varphi_{1,r}\frac{\sum_1^N m_x \varphi_{1,x}}{\sum_1^N m_x \varphi_{1,x}^2} \quad (6)$$

where m_x is the seismic mass at story x, $\varphi_{1,x}$ is the first-mode amplitude at story x, $\varphi 1,r$ is the first-mode amplitude at the roof level, and N denotes the total number of stories. The calculated overstrength and ductility parameters were subsequently used to compare the seismic performance characteristics of the archetype frames designed according to the two seismic design standards.

The pushover curves obtained for all archetype structures are presented in Figure 8. The seismic performance parameters extracted from these curves are summarized in Table 4, while a direct comparison between the ASCE 7-22 and NBCC 2020 designs is provided in Figure 9. As expected, the design periods and effective seismic weights of the corresponding archetypes designed according to the two standards are relatively close, indicating that the considered structures possess similar global characteristics.

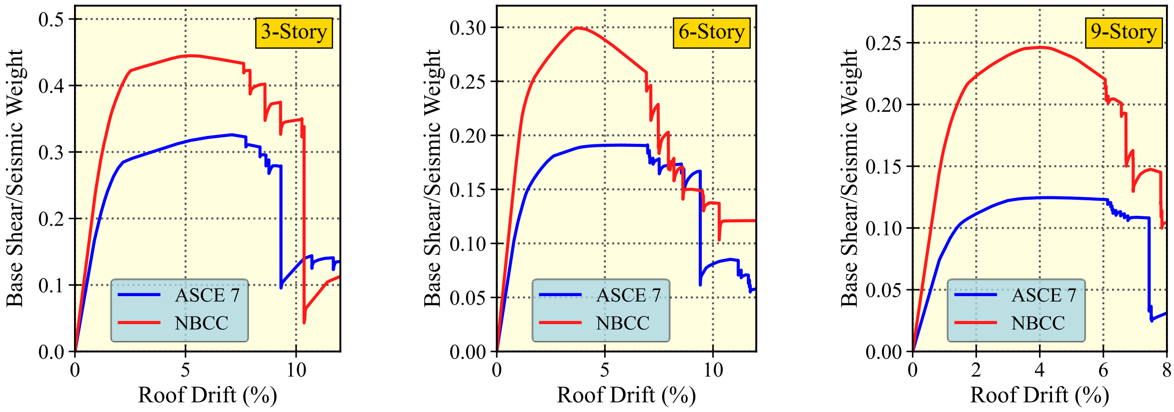

Figure 8. Normalized pushover curves of the archetype frames designed according to ASCE 7-22 and NBCC 2020.

Compared with the ASCE 7-22 frames, the NBCC 2020 archetypes generally developed higher initial stiffness and larger peak base shear (V_{max}). This behavior is primarily attributed to the larger member sections required by the NBCC design provisions, which resulted in greater lateral strength. Consequently, the calculated overstrength factors (Ω) were consistently higher for the NBCC frames. On the other hand, the ASCE 7-22 designs exhibited greater ductility (μ_T), indicating a larger deformation capacity after yielding.

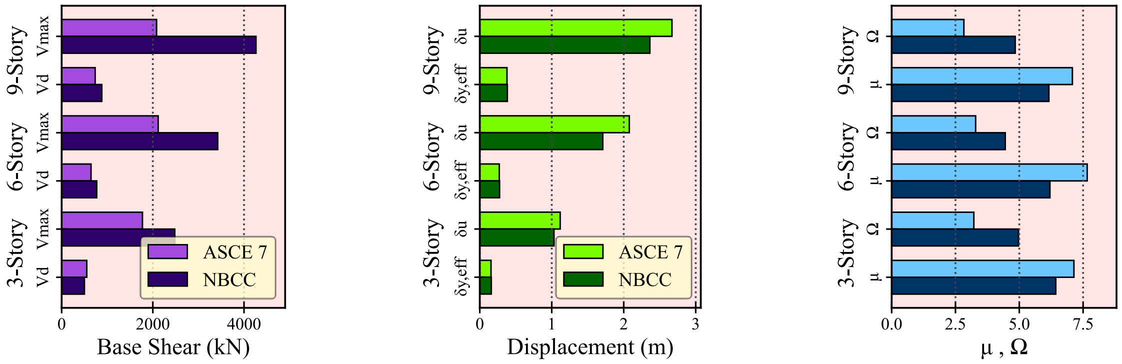

Figure 9. Comparison of seismic performance parameters obtained from pushover analyses

Another important aspect investigated in this study is the sequence and distribution of plastic hinge formation within the archetype frames. Understanding the development of plastic hinges provides valuable insight into the effectiveness of the seismic design and the ability of the structure to achieve the intended inelastic response mechanism. The progression of plastic hinge formation for all archetype structures is illustrated in Figure 10.

Table 4. Seismic performance parameters obtained from nonlinear pushover analyses.

Model	Code	αT (s)	T_a (s)	W (kN)	V_d (kN)	V_{max} (kN)	$\delta_{y,eff}$ (m)	δ_u (m)	μ_T	Ω_0
3-Story	ASCE 7	0.74	1.23	5438.78	550.99	1772.17	0.156	1.117	7.14	3.22
	NBCC	0.82	1.06	5579.47	499.31	2481.44	0.160	1.031	6.43	4.97
6-Story	ASCE 7	1.35	2.11	11074.28	644.37	2117.00	0.271	2.077	7.66	3.29
	NBCC	1.38	1.69	11436.45	769.10	3422.83	0.275	1.709	6.20	4.45
9-Story	ASCE 7	1.78	3.11	16709.52	735.22	2082.17	0.378	2.670	7.08	2.83
	NBCC	1.87	2.21	17312.58	880.71	4262.63	0.383	2.363	6.16	4.84

Note: α represents the code-specified period limit coefficient, equal to 1.5 in NBCC 2020 and 1.4 in ASCE 7-22.

Figure 10 shows that plastic hinges were primarily concentrated at the beam ends and at the bases of the first-story columns, which is consistent with the expected response of high-ductility steel moment-resisting frames. This response confirms that the strong-column weak-beam design philosophy was successfully achieved and that inelastic deformations were concentrated in the intended yielding regions. Consequently, the formation pattern of plastic hinges indicates satisfactory seismic performance and appropriate structural design. For the three- and six-story archetypes, plastic hinges generally initiated in the lower stories and gradually propagated upward as the lateral displacement increased. In contrast, the nine-story frames exhibited a different response pattern, where yielding first developed in the intermediate stories before extending toward the lower levels of the structure. It is also noteworthy that, for the six-story frame designed according to ASCE 7-22, a plastic hinge developed in columns located at an intermediate story. Such behavior is generally undesirable because it indicates partial violation of the intended beam-sway mechanism and may increase the likelihood of story instability. In comparison, no intermediate-story column hinging was observed in the corresponding NBCC-designed frame, suggesting a more favorable distribution of inelastic demands and improved adherence to the strong-column weak-beam philosophy.

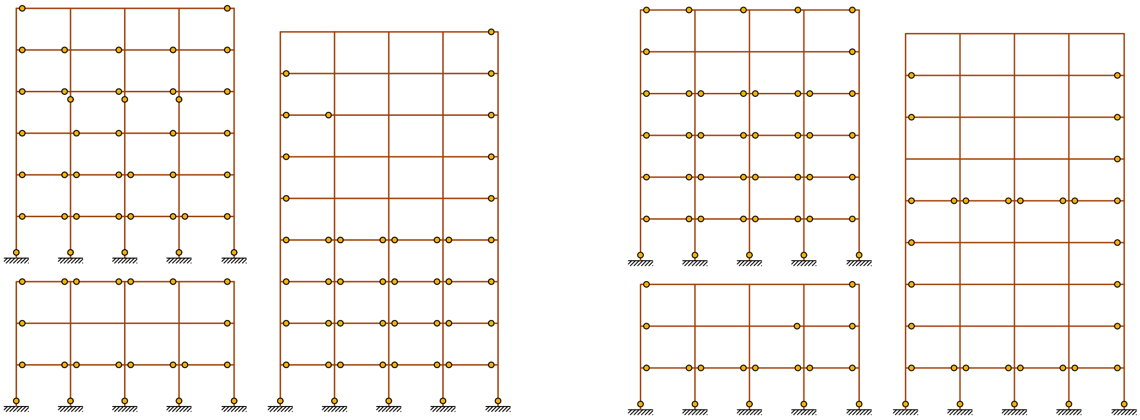

Figure 10. Distribution of plastic hinge formation in the archetype frames obtained from nonlinear pushover analyses.

4.2. Pushdown analysis procedure

The resistance of the archetype frames against progressive collapse was evaluated using nonlinear static pushdown analysis. Unlike conventional pushover analysis, where lateral loads are incrementally applied, pushdown analysis imposes a gradually increasing vertical displacement at the location of the removed column. The resulting load–displacement relationship provides valuable insight into the load redistribution mechanisms, reserve strength, and collapse resistance of the structural system following local damage.

In the present study, the pushdown analysis was performed using a displacement-controlled procedure. After the selected column was removed from the analytical model, a monotonically increasing downward displacement was imposed at the location of the removed column until a sufficiently large deformation level was achieved. Compared with force-controlled approaches, displacement-controlled analysis allows the complete structural response to be captured, including post-peak behavior and potential strength degradation [10].

The nonlinear static pushdown procedure adopted in this study has been used for progressive-collapse assessment (e.g., Kim et al. [10]) because it efficiently captures structural nonlinear behavior without requiring computationally intensive nonlinear dynamic analyses. Following the General Services Administration (GSA) guideline [31], amplified gravity loading was adopted to approximately account for dynamic amplification; however, the dynamic effects associated with sudden column removal are not explicitly captured and should be recognized as a limitation of the adopted methodology.

For the progressive collapse assessment, the gravity loading followed the GSA recommendations. In contrast to the nonlinear pushover analysis, where the gravity load combination of D+0.25L was applied, the gravity loads acting on the spans directly affected by the removed column were amplified to 2(D+0.25L). This amplification is intended to approximately account for the dynamic effects associated with the sudden loss of a primary load-carrying member. The application of this loading condition is illustrated in Figure 11. As can be observed, the amplified gravity load was applied to all floors within the bay associated with the removed column, while the remaining portions of the structure retained the conventional gravity loading.

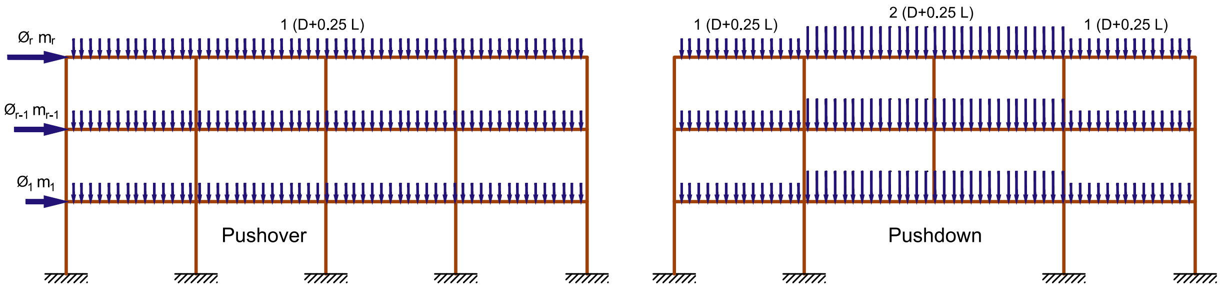

Figure 11. Gravity loading configuration adopted for the pushdown analyses according to the GSA guidelines.

To investigate the influence of column location on the collapse resistance of the structures, two column-removal scenarios were considered in this study. Case 1 corresponds to the removal of an interior column, whereas Case 2 represents the removal of an exterior column. Interior and exterior column removal were selected because they represent the most critical damage scenarios commonly considered in progressive-collapse assessment. As recommended by the GSA guidelines, an element was assumed to have reached its failure state when its plastic rotation reached 0.035 rad.

Figures 12 and 13 present the normalized pushdown load–displacement responses of the archetype frames subjected to the interior-column removal (Case 1) and exterior-column removal (Case 2) scenarios, respectively, where the vertical load is normalized by the applied GSA gravity loading (P/[2(D+0.25L)]). The quantitative results of the pushdown analyses are summarized in Table 5. In both cases, the frames designed according to NBCC exhibit substantially higher initial stiffness, peak load capacity, and post-yield resistance than their ASCE 7 counterparts. The difference becomes more pronounced as the building height increases, indicating the beneficial effect of the larger member sizes and higher steel weight associated with the NBCC-designed frames. For the 3-, 6-, and 9-story structures, the maximum pushdown resistance of the NBCC models is consistently about two times greater than that of the corresponding ASCE 7 models.

Table 5. Quantitative results of the pushdown analyses.

Scenario	model	Design Code	Peak Load (kN)	Displacement At Peak Load (m)	Displacement At Failure (m)
Case 1	3-Story	ASCE 7	230	0.165	0.185
	3-Story	NBCC	570	0.205	0.240
	6-Story	ASCE 7	1300	0.225	0.235
	6-Story	NBCC	2020	0.220	0.240
	9-Story	ASCE 7	2050	0.180	0.230
	9-Story	NBCC	5250	0.215	0.285
Case 2	3-Story	ASCE 7	110	0.150	0.160
	3-Story	NBCC	280	0.205	0.245
	6-Story	ASCE 7	630	0.215	0.235
	6-Story	NBCC	1000	0.225	0.275
	9-Story	ASCE 7	1020	0.200	0.245
	9-Story	NBCC	2580	0.210	0.285

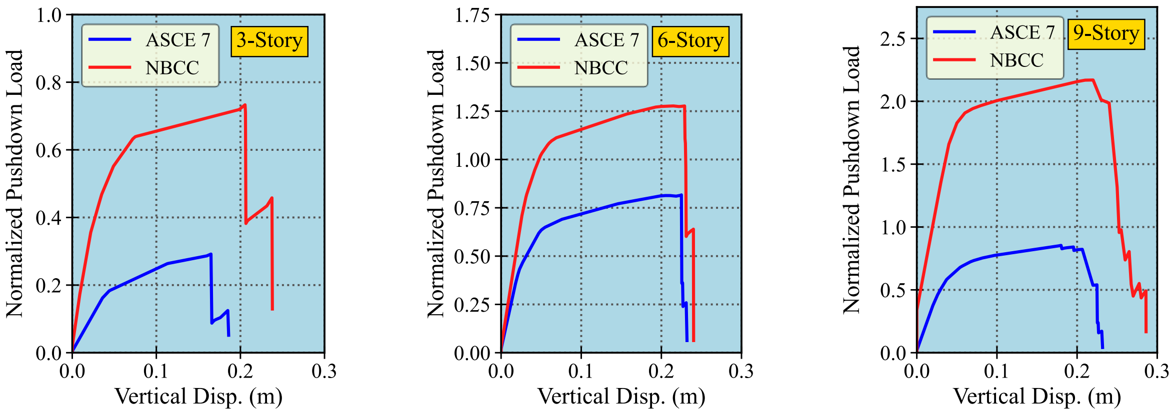

Figure 12. Pushdown load–displacement curves for the interior column removal scenario (Case 1).

A comparison between the two column-removal scenarios shows that the interior-column removal case generally develops considerably larger load-carrying capacities than the exterior-column removal case. This behavior can be attributed to the existence of alternative load-transfer paths on both sides of the removed interior column, which allows the surrounding beams and columns to mobilize stronger frame action and more effective load redistribution. In contrast, the exterior-column removal scenario provides fewer redistribution paths, resulting in lower resistance and earlier strength degradation. Although the ultimate vertical displacement capacities of the two cases are relatively similar, the interior-column removal scenario exhibits a more stable post-peak response and greater energy dissipation capacity, particularly for the mid-rise and high-rise frames. Overall, among the investigated damage scenarios, the interior-column removal case demonstrates superior redundancy and collapse resistance due to its more effective load redistribution mechanism.

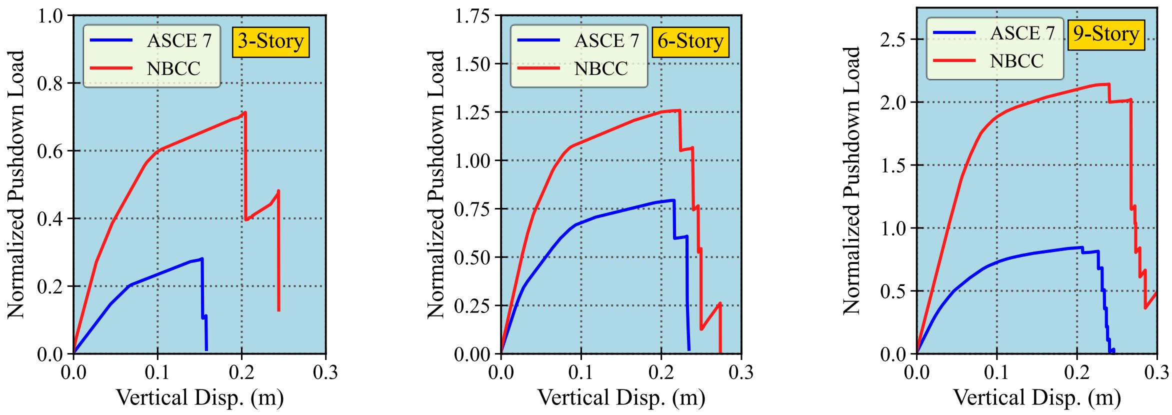

Figure 13. Pushdown load–displacement curves for the exterior column removal scenario (Case 2).

Figure 14 illustrates the sequence and distribution of plastic hinge formation obtained from the pushdown analyses for both column-removal scenarios. For clarity, only one set of hinge patterns is presented, since the ASCE 7 and NBCC models exhibited nearly identical collapse mechanisms and hinge formation sequences. As observed, plastic hinges primarily develop at the ends of the beams adjacent to the removed column, indicating that these members play the dominant role in redistributing gravity loads after column loss. The progression of yielding generally initiates in the lower stories and subsequently propagates toward the upper levels as the imposed vertical displacement increases. This pattern demonstrates the ability of the surrounding frame members to develop alternative load-transfer paths and mobilize additional resistance mechanisms during the progressive collapse process.

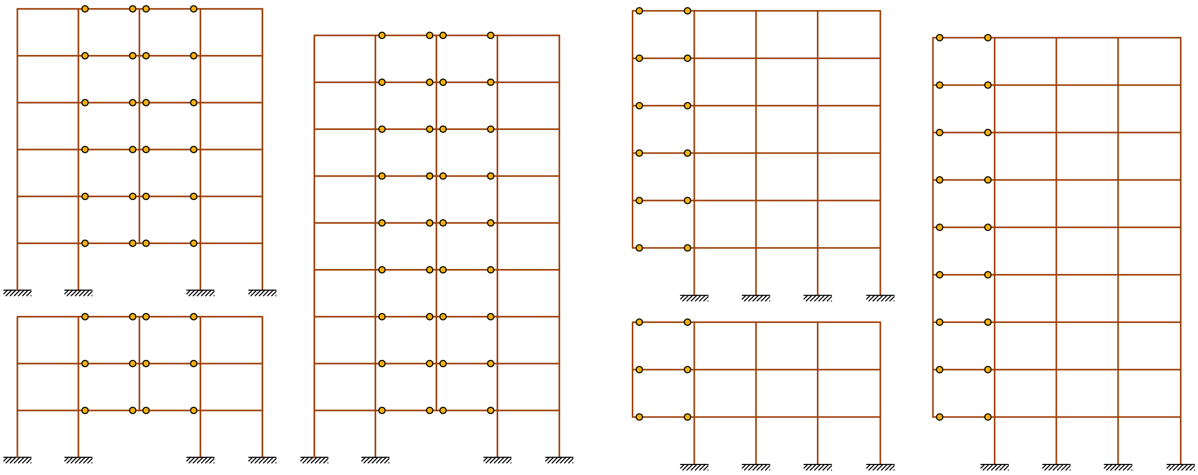

Figure 14. Plastic hinge formation patterns obtained from pushdown analyses under the investigated column-removal scenarios.

5. Summary and Conclusions

This study investigated the influence of seismic design provisions on the seismic and progressive collapse performance of high-ductility steel moment-resisting frames designed according to ASCE 7-22 and NBCC 2020. Three-, six-, and nine-story archetype frames were designed in ETABS following the requirements of AISC 360-22, AISC 341-22, and CSA S16-19, and subsequently modeled in OpenSees for nonlinear analyses. Nonlinear pushover analyses were performed to evaluate the seismic capacity, overstrength, ductility, and plastic hinge development of the structures, while nonlinear pushdown analyses were conducted to assess their resistance against progressive collapse under interior- and exterior-column removal scenarios. Based on the obtained results, the following conclusions can be drawn:

A comparison of the design story shear distributions revealed that the ASCE 7-22 archetype exhibited slightly higher story shear demands than the corresponding NBCC 2020 design in the three-story frame. However, for the six- and nine-story archetypes, the NBCC-designed frames generally developed larger story shear forces throughout the building height.

The frames designed according to NBCC 2020 required approximately 1.5 times more structural steel than their ASCE 7-22 counterparts. This difference is primarily attributed to the more stringent drift-control provisions prescribed by the Canadian code.

The nonlinear pushover analyses showed that the NBCC-designed frames consistently exhibited higher initial stiffness than the corresponding ASCE-designed archetypes. The maximum base shear capacity (V_{max}) and overstrength factor (Ω) obtained from the pushover analyses were greater for all NBCC-designed frames, reflecting their enhanced lateral load-carrying capacity. In contrast, the ASCE 7-22 archetypes demonstrated larger period-based ductility factors (μ_T), indicating a greater ability to sustain inelastic deformations before reaching their ultimate limit state.

The plastic hinge formation patterns obtained from the pushover analyses confirmed that yielding was concentrated primarily at beam ends and first-story column bases, demonstrating satisfactory compliance with the strong-column weak-beam design philosophy in most cases. However, limited intermediate-story column hinging was observed in the six-story ASCE 7-22 frame.

For the selected deterministic archetypes, spectra, 2D modeling assumptions, and static pushdown procedure adopted in this study, the NBCC-designed frames exhibited substantially greater progressive-collapse resistance than the corresponding ASCE 7-22 frames. This behavior was primarily attributed to the larger member sizes and higher steel consumption required by the NBCC design provisions. Consequently, for all investigated building heights, the maximum pushdown load capacity of the NBCC archetypes was approximately twice that of the ASCE-designed models.

Comparison of the column-removal scenarios showed that the interior-column removal case developed substantially higher load-carrying capacity and a more stable post-peak response than the exterior-column removal case due to the presence of alternative load-transfer paths on both sides of the removed column.

The plastic hinge patterns obtained from the pushdown analyses indicated that yielding was concentrated mainly at the ends of beams adjacent to the removed column and progressively spread to upper stories as the imposed vertical displacement increased. Furthermore, the ASCE 7-22 and NBCC 2020 models exhibited nearly identical collapse mechanisms and hinge formation sequences.

Finally, it should be noted that progressive-collapse behavior may be influenced by several structural and modeling parameters, including material properties, connection behavior, gravity-load assumptions, damping, plastic rotation capacity, span length, story height, and building height. Although some of these aspects have been investigated in previous studies, a comprehensive evaluation of their influence, together with three-dimensional effects, slab/composite action, and nonlinear dynamic column-removal analysis, is beyond the scope of the present study and represents a valuable direction for future research.

Nomenclature

ASCE	American Society of Civil Engineers
NBCC	National Building Code of Canada
CSA	Canadian Standards Association
AISC	American Institute of Steel Construction
MRF	Moment-Resisting Frame
SMF	Special Moment Frame
D-MRF	Ductile Moment-Resisting Frame
GSA	General Services Administration
IMK	Ibarra–Medina–Krawinkler deterioration model
(D)	Dead load
(L)	Live load
(V)	Base shear
(W)	Seismic weight of the structure
(V/W)	Normalized base shear
P–Δ	Second-order geometric effect
SCWB	Strong-Column Weak-Beam

Declaration of Conflict of Interests

The authors declare that there is no conflict of interest. They have no known competing financial interests or personal relationships that could have appeared to influence the work reported in this paper.

References

[1.] Flores FX, Charney FA, Lopez-Garcia D. Influence of the gravity framing system on the collapse performance of special steel moment frames. J Constr Steel Res 2014; 101:351–62. https://doi.org/10.1016/j.jcsr.2014.05.020.

[2.] Özhendekci D, Özhendekci N. Seismic performance of steel special moment resisting frames with different span arrangements. J Constr Steel Res 2012; 72:51–60. https://doi.org/10.1016/j.jcsr.2011.10.002.

[3.] Aslani M, Tavousi Tafreshi S, Gorji Azandariani M. Seismic resilience assessment of moment-resisting frames equipped with novel hybrid rotational friction damper and SMA cables. Structures 2026; 84:110976. https://doi.org/10.1016/j.istruc.2025.110976.

[4.] Flores FX, Lopez-Garcia D, Charney FA. Assessment of floor accelerations in special steel moment frames. J Constr Steel Res 2015; 106:154–65. https://doi.org/10.1016/j.jcsr.2014.12.006.

[5.] Shi Y-A, Liu G, Liang Y-J, He X, Cui K-Y, Xu R-H. Experimental study on the cyclic behavior of high-performance weathering steel connections in moment-resisting frames. Structures 2026; 87:111690. https://doi.org/10.1016/j.istruc.2026.111690.

[6.] Heshmati M, Khatami A, Shakib H. FEMA P695 methodology for safety margin evaluation of steel moment resisting frames subjected to near-field and far-field records. SN Appl Sci 2021;3. https://doi.org/10.1007/s42452-021-04230-2.

[7.] Jayarajan P. Seismic Assessment of Steel Moment Resisting Frames with Partial-Strength Connections, 2025, p. 381–93. https://doi.org/10.1007/978-981-97-6067-1_37.

[8.] Lignos DG, Hikino T, Matsuoka Y, Nakashima M. Collapse Assessment of Steel Moment Frames Based on E-Defense Full-Scale Shake Table Collapse Tests. Journal of Structural Engineering 2013; 139:120–32. https://doi.org/10.1061/(ASCE)ST.1943-541X.0000608.

[9.] Galvis, F. A., Deierlein, G. G., Molina Hutt, C., Issa, O., Baker, J. W., & Zsarnóczay, A. (2022). Seismic assessment of pre-Northridge welded steel moment frame buildings and implications on community resilience.

[10.] Kim T, Kim J, Park J. Investigation of Progressive Collapse-Resisting Capability of Steel Moment Frames Using Push-Down Analysis. Journal of Performance of Constructed Facilities 2009; 23:327–35. https://doi.org/10.1061/(ASCE)0887-3828(2009)23:5(327).

[11.] Liu Y, Ma L, Ye H, Wei Z, Zhao K, Li G. Synergistic enhancement of seismic and progressive collapse resistance in prefabricated RCS frame structures. Journal of Building Engineering 2026; 125:116157. https://doi.org/10.1016/j.jobe.2026.116157.

[12.] Li H-H, Bei J-L, Yu Z-W, Zhang J-Z. Progressive collapse resistance of 3D steel frames with floor slabs under an interior column removal scenario: Test and analysis. Eng Struct 2026; 361:122927. https://doi.org/10.1016/j.engstruct.2026.122927.

[13.] Song M, Wang Z, Chen X, Huang S, Liu B, He J. Experimental investigation and theoretical analysis on progressive collapse performance of fully bonded prestressed precast concrete frames. Journal of Building Engineering 2026; 127:116362. https://doi.org/10.1016/j.jobe.2026.116362.

[14.] Elshaer A, Mostafa H, Salem H. Progressive collapse assessment of multistory reinforced concrete structures subjected to seismic actions. KSCE Journal of Civil Engineering 2017; 21:184–94. https://doi.org/10.1007/s12205-016-0493-6.

[15.] Al-Salloum YA, Abbas H, Almusallam TH, Ngo T, Mendis P. Progressive collapse analysis of a typical RC high-rise tower. Journal of King Saud University - Engineering Sciences 2017; 29:313–20. https://doi.org/10.1016/j.jksues.2017.06.005.

[16.] Zhao X, Yan S, Chen Y. Comparison of progressive collapse resistance of single-layer latticed domes under different loadings. J Constr Steel Res 2017; 129:204–14. https://doi.org/10.1016/j.jcsr.2016.11.012.

[17.] ASCE/SEI 7–22, Minimum Design Loads and Associated Criteria for Buildings and Other Structures, American Society of Civil Engineers, Reston, Virginia, 2022.

[18.] National Research Council of Canada. (2020). National Building Code of Canada 2020. National Research Council Canada.

[19.] ANSI/AISC 360–22, Specification for Structural Steel Buildings, American Institute of Steel Construction, Chicago, Illinois, 2022.

[20.] ANSI/AISC 341–22, Seismic Provisions for Structural Steel Buildings, American Institute of Steel Construction, Chicago, Illinois, 2022.

[21.] Canadian Standards Association. (2019). CSA S16:19—Design of steel structures. CSA Group.

[22.] ETABS. (2022). Structural software for building analysis and design. Berkeley, California, USA: Computers and Structures, Inc.

[23.] McKenna F. OpenSees: A Framework for Earthquake Engineering Simulation. Comput Sci Eng 2011; 13:58–66. https://doi.org/10.1109/MCSE.2011.66.

[24.] Guidelines for nonlinear structural analysis and design of buildings. part IIa - steel moment frames. Gaithersburg, MD: 2017. https://doi.org/10.6028/NIST.GCR.17-917-46v2.

[25.] Ibarra LF, Medina RA, Krawinkler H. Hysteretic models that incorporate strength and stiffness deterioration. Earthq Eng Struct Dyn 2005; 34:1489–511. https://doi.org/10.1002/eqe.495.

[26.] Ibarra LF, Krawinkler H. Global collapse of frame structures under seismic excitations. The John A. Blume Earthquake Engineering Center, Stanford University, Stanford, CA. Rep. No. TB 152, 2005.

[27.] Lignos DG, Krawinkler H. Deterioration Modeling of Steel Components in Support of Collapse Prediction of Steel Moment Frames under Earthquake Loading. Journal of Structural Engineering 2011; 137:1291–302. https://doi.org/10.1061/(ASCE)ST.1943-541X.0000376.

[28.] Hartloper, A., and Lignos, D.G., 2016, Updates to the ASCE-41-13 Nonlinear Modeling Provisions for Performance-Based Seismic Assessment of New and Existing Steel Moment Resisting Frames, M.Eng., Thesis, McGill University, Montreal, Canada.

[29.] NEHRP Consultants Joint Venture, Evaluation of the FEMA P-695 Methodology for Quantification of Building Seismic Performance Factors, NIST GCR 10-917-8, National Institute of Standards and Technology, Gaithersburg, MD, 2010.

[30.] FEMA P695. Quantification of Building Seismic Performance Factors. Washington DC: Federal Emergency Management Agency; 2009.

[31.] U.S. General Services Administration. (2016). Alternate path analysis and design guidelines for progressive collapse resistance (2016 ed.). Office of the Chief Architect, U.S. General Services Administration.

How to Cite This Article

Mirzaei, A., Bargi, K., Progressive Collapse and Structural Resistance Assessment of Code-Compliant High-Ductility Steel MRFs under NBCC and ASCE 7, Civil Engineering Beyond Limits, 4(2026), 11154.
https://doi.org/10.36937/cebel.2026.11154